Pflügers Archiv - European Journal of Physiology (2021) 473:507–519
https://doi.org/10.1007/s00424-020-02507-w

ORIGINAL ARTICLE

Pathological activation of CaMKII induces arrhythmogenicity through TRPM4 overactivation

Yaopeng Hu[1] · Daniela Ross Kaschitza[2] · Maria Essers[2] · Prakash Arullampalam[2] · Takayuki Fujita[1] · Hugues Abriel[2] · Ryuji Inoue[1]

Received: 29 September 2020 / Revised: 2 December 2020 / Accepted: 16 December 2020 / Published online: 4 January 2021

Abstract

TRPM4 is a Ca^{2+}-activated nonselective cation channel involved in cardiovascular physiology and pathophysiology. Based on cellular experiments and numerical simulations, the present study aimed to explore the potential arrhythmogenicity of CaMKII-mediated TRPM4 channel overactivation linked to Ca^{2+} dysregulation in the heart. The confocal immunofluorescence microscopy, western blot, and proximity ligation assay (PLA) in HL-1 atrial cardiomyocytes and/or TRPM4-expressing TSA201 cells suggested that TRPM4 and CaMKII proteins are closely localized. Co-expression of TRPM4 and CaMKIIδ or a FRET-based sensor *Camui* in HEK293 cells showed that the extent of TRPM4 channel activation was correlated with that of CaMKII activity, suggesting their functional interaction. Both expressions and interaction of the two proteins were greatly enhanced by angiotensin II treatment, which induced early afterdepolarizations (EADs) at the repolarization phase of action potentials (APs) recorded from HL-1 cells by the current clamp mode of patch clamp technique. This arrhythmic change disappeared after treatment with the TRPM4 channel blocker 9-phenanthrol or CaMKII inhibitor KN-62. In order to quantitatively assess how CaMKII modulates the gating behavior of TRPM4 channel, the ionomycin-permeabilized cell-attached recording was employed to obtain the voltage-dependent parameters such as steady-state open probability and time constants for activation/deactivation at different $[Ca^{2+}]_i$. Numerical simulations incorporating these kinetic data into a modified HL-1 model indicated that > 3-fold increase in TRPM4 current density induces EADs at the late repolarization phase and CaMKII inhibition (by KN-62) completely eliminates them. These results collectively suggest a novel arrhythmogenic mechanism involving excessive CaMKII activity that causes TRPM4 overactivation in the stressed heart.

Keywords TRP channel · Arrhythmogenicity · Ca dynamics · Simulation

Introduction

Cardiac arrhythmia is a common disease with high morbidity and mortality in the developed world, some of which is still intractable lacking effective treatments. Electrical and structural remodeling has been regarded as one of crucial processes of arrhythmogenesis, where aberrant calcium signaling and downstream mechanisms play pivotal roles [12].

Recently, transient receptor potential (TRP) channels have attracted growing attention because of their involvement in many stress-induced dysfunctions including cardiac arrhythmias [15]. A notable example is a melastatin subfamily member, a Ca^{2+}-activated nonselective cation channel TRPM4. TRPM4 is ubiquitously expressed in the heart, most abundantly in the atrium and conduction system. Besides some hereditary arrhythmias (familial AV block, Brugada syndrome), TRPM4 is responsible for secondary arrhythmic changes in

Contributions to Special Issues This article is published as part of the Special Issue on Calcium Signal Dynamics in Cardiac Myocytes and Fibroblasts: Mechanisms and Therapeutics.

This article is part of the special issue on Calcium Signal Dynamics in Cardiac Myocytes and Fibroblasts: Mechanisms in Pflügers Archiv—European Journal of Physiology

✉ Yaopeng Hu
huyaopeng@fukuoka-u.ac.jp

✉ Ryuji Inoue
inouery@fukuoka-u.ac.jp

[1] Department of Physiology, Fukuoka University School of Medicine, 7-45-1 Nanakuma, Jonan-ku, Fukuoka 814-0180, Japan

[2] Institute of Biochemistry and Molecular Medicine, National Center of Competence in Research NCCR TransCure, University of Bern, Bern, Switzerland

the remodeled or injured hearts, such as action potential (AP) prolongation, early afterdepolarization (EAD), and presumably delayed afterdepolarization (DAD) [11, 27]. These changes result from the predominance of inward over outward currents, due to reduced K^+ currents, increased inward currents (e.g., sustained Na^+ currents, reactivation of Ca^{2+} currents), or both. TRPM4 may act as an additional but non-trivial inward current contributing to the slow pre-upstroke depolarization and late repolarization phases of AP [13, 14].

During structural and electrical remodeling of the heart, Ca^{2+}/calmodulin-dependent kinase II (CaMKII) plays multifaceted roles in a diverse array of pathological processes including aberrant excitation and transcription [3]. Sustained activation of CaMKII occurs in response to abnormal cytosolic Ca^{2+} rise, which persists independently of Ca^{2+}/calmodulin through auto-phosphorylation, angiotensin II (AGII)-induced oxidation, glycosylation in diabetic conditions, and NO-mediated S-nitrosylation during β-adrenergic stimulation [21]. CaMKII-mediated phosphorylation has been shown to be central to DAD-related atrial fibrillation [25]. In our former experiments in HL-1 cells, AGII treatment remarkably enhanced TRPM4 activity, causing AP prolongation and EAD [16]. In some case, large diastolic depolarizations accompanying spontaneous AP activities also occurred (unpublished observations). It is thus tempting to assume a causal relationship between enhanced CaMKII and TRPM4 activities and its pathophysiological implications in arrhythmogenesis.

In the present study, we investigated how excessive CaMKII activation affects TRPM4 channel activity to induce arrhythmogenicity under altered Ca^{2+} handling. To address this issue, we firstly explored the interaction between TRPM4 and CaMKII proteins by different methodological approaches. We then mathematically formulated CaMKII-mediated modulation of TRPM4 channel gating to perform numerical AP simulations and compared the results with electrophysiological data obtained from HL-1 cells.

Methods

Cell culture and gene transfection

Human embryonic kidney cells (HEK293) or TSA201 cells (ATCC, USA) were maintained in Dulbecco's modified Eagle medium (DMEM) supplemented with 10% fetal bovine serum (FBS) and antibiotics under humidified, 5% CO_2-gassed conditions and passaged every 3–4 days. No specific differences were however found between these two cell lines. For heterologous expression of TRPM4 and CaMKII, the cells were transfected with human *trpm4b* cDNA (pCIneo vector; originally provided by Jean-Pierre Kinet and Pierre Launay) and pDONR223-CaMKIIδ (Addgene #23814, a gift from William Hahn and David Root) [19] by the aid of LipoD293™ (SignaGen, SL100668), and used for electrophysiological measurements 24–48 h later.

An immortalized atrial cardiomyocyte line HL-1 (originally provided by William C. Claycomb) was maintained in a special culture medium (Claycomb Medium; Sigma-Aldrich #51800C) according to the optimized protocol provided by Claycomb's laboratory [6]. HL-1 cells were treated with angiotensin II (1 μM) for 72–96 h before patch clamp experiments.

Immunofluorescence

HL-1 cells were seeded on pre-coated cover slips and cultured in Claycomb's medium supplemented with 10% FBS. The cells were incubated with AGII for 4 days. After washing once with phosphate-buffered saline (PBS), the cells were fixed with 4% para-formaldehyde for 15 min at room temperature. Subsequently, they were permeabilized and blocked for 60 min with blocking solution (1× PBS/5% normal serum/0.3% Triton™ X-100), then immunolabelled. The mouse monoclonal anti-CaMKII (Invitrogen, MA5-27735) and rabbit polyclonal anti-TRPM4 (Pineda, Germany) antibodies were used as the primary antibodies. For the secondary antibodies, the anti-mouse antibody labelled with Alexa Fluor 488 (Cell Signaling, 4408S) and the anti-rabbit antibody labelled with Alexa Fluor 568 (Invitrogen, A-11036) were applied. After rinsing with PBS, the cover slips were mounted with the medium containing 4′,6-diamidino-2-phenylindole (DAPI). A laser-scanning confocal microscope (LSM 880, ZEN 2.1, Zeiss, Oberkochen, Germany) was used to detect the immunofluorescences from Alexa Fluor 488, Alexa Fluor 568, and DAPI.

Proximity ligation assay

The Duolink® (Sigma, USA) proximity ligation assay (PLA) was performed in both HL-1 and transfected TSA-201 cells, according to the literature [26] as well as the manufacturer's recommendations. The PLA assay is a powerful tool for the in situ detection of proteins located in close proximity (< 40 nm). HL-1 or TSA-201 cells were fixed by blocking solution then incubated with primary antibodies. After washing three times with PBS, secondary antibodies conjugated to PLA probes were added on the cells for 1-h incubation. The PLA probes are oligonucleotide pairs that if only in close proximity hybridize to form a closed circular DNA and then act as the template primers for rolling circle amplification. Thereafter, cell samples on cover slips were mounted with the Duolink in situ mounting medium with DAPI and viewed by confocal microscopy. Samples without primary antibodies were taken as negative controls. Images were analyzed by the Duolink® ImageTool (Sigma).

Western blot

Total cell lysates from HL-1 cells were homogenized in RIPA buffer with protease inhibitors on ice. The protein concentration was measured by using the XL-Bradford protein assay kit (APRO SCIENCE, Japan). The yielded proteins were boiled in Laemmli sample buffer with 5% (v/v) 2-mercaptoethanol and 1% (w/v) bromophenol blue, separated by 10% (w/v) SDS-PAGE and electrophoretically transferred to a PVDF membrane. The membrane was blocked with Blocking One Buffer (Nacalai Tesque, Japan), and then incubated with anti-TRPM4 antibody (Abcam, ab106200, diluted 1:200), anti-CaMKII (SANTA CRUZ, sc-5306, diluted 1:200), or anti-β-actin (Cell Signaling, 4967S, diluted 1:1000). Protein expression levels were evaluated by the LAS-3000 Imaging System (Fujifilm, Japan) after incubating the membrane with the secondary antibody linked to horseradish peroxidase.

Förster resonance energy transfer

To evaluate CaMKII activity, fluorescent CaMKII indicator pcDNA3-*Camui*-CR (Addgene #40256, a gift from Michael Lin) [20] was co-expressed into HEK293 cells. *Camui* fluorescence was measured as the Förster resonance energy transfer (FRET) efficiency. Firstly, excitation lights filtered at 430 ± 10 nm was applied from a computer-controlled high-speed wavelength-switching light source (Lambda DG-4, Sutter Instrument Co., Novato, CA). Epifluorescence was pre-filtered through a multi-band dichroic mirror contained in the microscope, and then separated and filtered in a beam splitter at 464 ± 23 nm (for donor fluorescence, F_{CFP}) and 542 ± 27 nm (for acceptor fluorescence, F_{YFP}). F_{YFP}/F_{CFP} fluorescence ratio normalized to basal level was assumed as the FRET singal of *Camui* that reflects CaMKII activity [2]. Data acquisition and analysis were implemented by the software MetaMorph v.7.7 (Molecular Devices, CA, USA).

Electrophysiology

For patch clamp experiments, heat-polished borosilicate glass electrodes (4–6 MΩ) were used. Membrane currents and potentials were recorded in the voltage clamp and current clamp modes respectively by a low-noise, high-impedance patch clamp amplifier (EPC10, HEKA Elektronik, Germany). Data analysis and illustration were made by using the commercially available software, Clampfit v.10. (Axon Instruments, USA), Labchart software v.7 (AD Instruments, Australia), and GraphPad Prism 8 (GraphPad Software, USA).

Solutions

Standard external solution used for patch clamp experiments consisted of the following (in mM): 140 NaCl, 5 KCl, 1.2 $MgCl_2$, 1.8 $CaCl_2$, 10 Hepes, 10 glucose (adjusted to pH 7.4 with Tris base). High-K^+ external solution for the Iono-C/A recording consisted of the following (in mM): 145 KCl, 1.2 $MgCl_2$, 0.1–5 $CaCl_2$, 10 Hepes, 10 glucose (adjusted to pH 7.4 with Tris base); internal (pipette) solution for current clamp recording (mM): 120 K glutamate, 20 KCl, K_2ATP, 2 $MgCl_2$, 10 Hepes, 1 Na_2EGTA (adjusted to pH 7.23 with Tris base); internal solution for the Iono-C/A recording: the standard external solution with 1 mM tetraethylammonium (TEA) and 100 μM 4,4′-diisothiocyano-2,2′-stilbenedisulfonic acid (DIDS) to block K and Cl channels. All drugs were applied via a custom-made fast solution change device "Y-tube" that was controlled by electrically driven solenoid valves [17]. Time required to complete solution change was ~ 1 s.

Numerical model simulation

For numerical simulation with a modified HL-1 evoked AP model, a free simulation software Cor1.1 (Oxford; URL: http://cor.physiol.ox.ac.uk/) was used. This model was modified so as to suppress the spontaneous activity by removing hyperpolarization-activated current and reducing the sensitivity (ESR50 = 0.4) and efficacy (ks = 25) of junctional Ca^{2+} release as well as halving the densities of voltage-dependent L-type and T-type Ca^{2+} channels in the original model with TRPM4 gating kinetics [16, 30]. The permeabilities P_{Na} and P_K for TRPM4 current in the HL-1 model, which correspond to the maximal conductances for Na^+ and K^+, were set to be $3.51*10^{-8}$ L/F/ms, respectively. These values were calculated from the maximum density of single TRPM4 channels endogenous to HL-1 cells determined by the inside-out patch recordings (under unstimulated conditions) as well as the whole cell and patch membrane capacitances (Fig. 4F and supplementary information in [16]). For Luo-Rudy 2000 ventricular AP model, a Ca^{2+}-activated nonselective cation current (NS_{Ca}) that was already defined in the model [16] was replaced by a TRPM4 current whose gating kinetics was characterized in detail in the previous and present studies. The pre-set values for $P_{NSCa,Na}$ and $P_{NSCa,K}$ in the original model ($1.75*10^{-7}$ L/F/ms for each) were employed. Ordinary differential equations in the model were numerically solved by the 4th-order Runge-Kutta algorithm, and APs and currents were iterated every 0.005 ms. For data illustration, simulated results were graphed in 1-ms resolution.

Statistical evaluation

All data are expressed as means ± s.e.m. Paired or unpaired Student's *t* tests were used for single comparison. ANOVA followed by Tukey's or Dunnett's post hoc tests were employed for multiple comparisons. $p < 0.05$ was taken statistically significant.

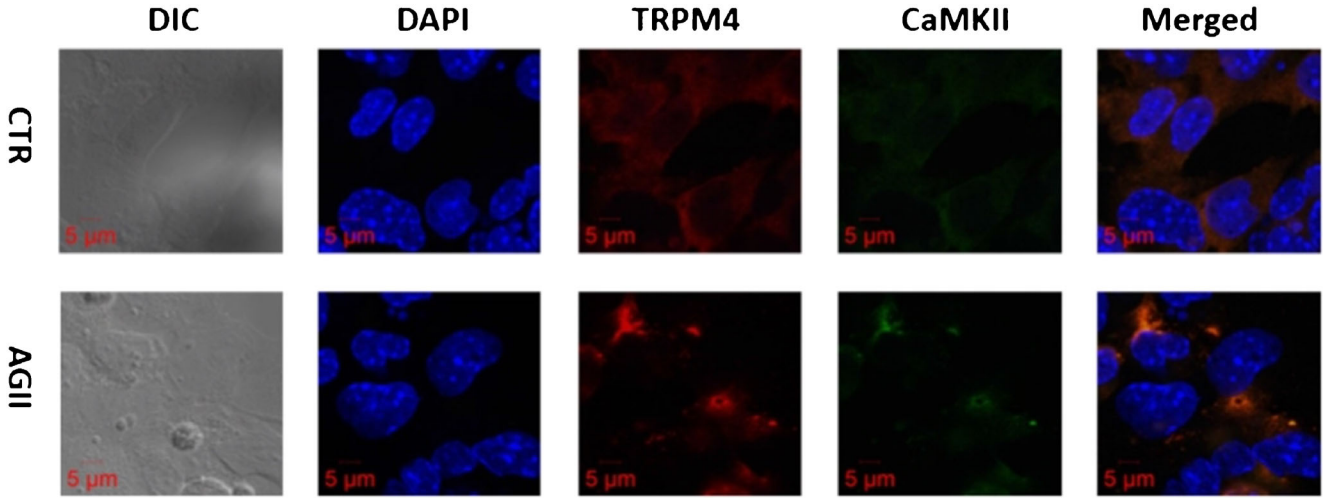

Fig. 1 Overlapped distribution of TRPM4 and CaMKII proteins is enhanced by AGII treatment. Confocal microscopy images of TRPM4 protein (red) and CaMKII (green) in HL-1 cells. Nuclei are stained with DAPI (blue). Rightmost columns: merged images: orange signals indicate the overlapped distributions of TRPM4 and CaMKII proteins. Note that the overlapped signals are stronger in strength and larger in number in AGII-treated (1 μM for 4 days) than in normal conditions. Data are representative of four different experiments

Results

Close localization of TRPM4 and CaMKII proteins in a heterologous expression system and HL-1 cardiomyocytes

At first, to examine the intracellular distribution of TRPM4 and CaMKII proteins in HL-1 cells, confocal immunofluorescence microscopy was carried out. Staining with polyclonal anti-TRPM4 and monoclonal anti-CaMKII antibodies produced predominantly cytosolic labelling. As indicated by the orange regions in merged images (upper rightmost in Fig. 1), fluorescent dye-labelled TRPM4 and CaMKII proteins were found to be closely localized. The degree of close localization was enhanced after 4-day incubation with AGII (lower rightmost in Fig. 1).

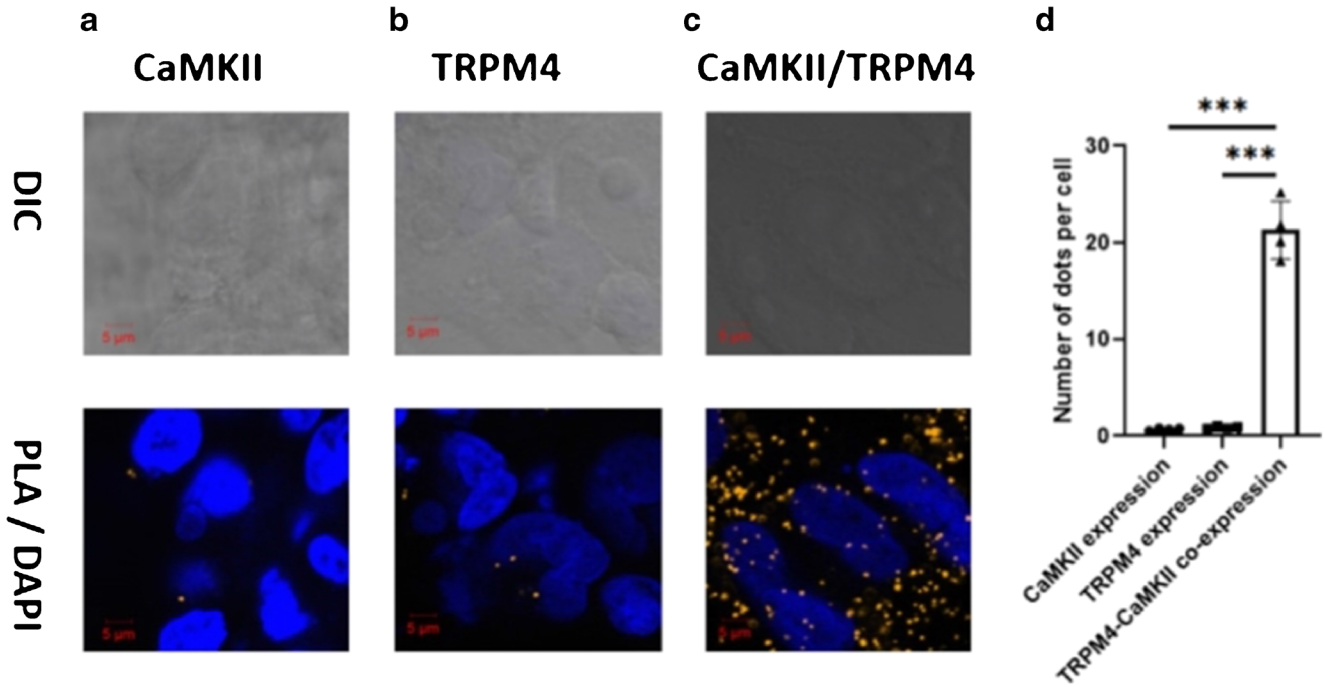

Fig. 2 Close localization of expressed TRPM4 with CaMKIIδ in TSA 201 cells. Representative PLA images from TSA 201 cells transiently transfected with either CaMKIIδ (**a**) or TRPM4 (**b**) proteins or co-expressed with both proteins together (**c**). Orange dot signals were generated when the distance of two proteins is within 40 nm. Nuclei are stained with DAPI in blue. Scale bars indicate 10 μm. (d) Quantitative analysis of the PLA signals. ***$p < 0.001$ with unpaired t test ($n = 4$)

To validate the above observations in situ, we next employed the proximity ligation assay (PLA). TSA201 cells were transfected with either CaMKIIδ or TRPM4 or both (Fig. 2a–c). In the figure, orange dots denote that the two proteins are present within 40 nm. While few signals were present with the sole expression of either CaMKIIδ or TRPM4, many orange dots appeared with TRPM4/CaMKIIδ co-expression (Fig. 2d). This strongly suggested that the two heterologously expressed proteins preferentially exist in close proximity to each other. The close localization of endogenous TRPM4 and CaMKIIδ proteins was also observed in non-transfected HL-1 cells by the PLA assay (Fig. 3b). Notably, incubation of HL-1 cells with AGII doubled the number of dot signals, facilitating the close localization of TRPM4 and CaMKII proteins (Fig. 3c, d).

Upregulation of TRPM4 and CaMKII accounts for arrhythmogenic changes in HL-1 cells

HL-1 cells retain many important features of cardiomyocytes with respect to intracellular signaling and expression of ion channels responsible for AP generation [32]. Expressions of both TRPM4 and CaMKII proteins in HL-1 cells were significantly increased after 4-day treatment with 1 μM angiotensin II (AGII) (Fig. 4a, b). The same procedure was found to cause several-fold increase in TRPM4 current density previously [16]. We tested whether the increased expressions of the two proteins induced by AGII are arrhythmogenic at the cellular level. With 2-Hz pacing, early afterdepolarizations (EADs) occurred much more frequently in AGII-treated than in non-treated HL-1 cells. Strikingly, inhibition of the activities of TRPM4 channel (by 10 μM 9-phenanthrol: 9-PA) and of CaMKII (by 5 μM KN-62) both significantly reduced the incidence of EAD (Fig. 4c, d). These results can be interpreted that excessive activities of TRPM4 and CaMKII are arrhythmogenic.

CaMKII positively regulates TRPM4 channel activity

In the next step, we explored the functional significance of CaMKII in regulating TRPM4 channel activity. For this purpose, we co-expressed TRPM4 and CaMKIIδ in HEK293 cells, and recorded TRPM4-mediated current by the ionomycin-permeabilized cell-attached (Iono-C/A) recording. This method allowed us to stably record the current over tens of seconds [16]. Only marginal currents were induced by externally administered Ca^{2+} after ionomycin permeabilization in mock-transfected HEK293 cells (data not shown). As shown in Fig. 5 a and c, administration of the CaMKII blocker KN-62 (5 μM) effectively inhibited TRPM4 currents induced by bath perfusion of Ca^{2+} after ionomycin permeabilization. These were paralleled by FRET changes reflecting CaMKII activity when a CaMKII sensor *Camui* was co-expressed (Fig. 5b, d; see the "Methods" section). These results strongly suggest that tight functional interaction may exist between CaMKII and TRPM4 proteins.

Kinetic analysis of TRPM4 channel modulation by CaMKII

To quantify CaMKII-mediated modulation of TRPM4 channel, we evaluated the voltage- and $[Ca^{2+}]_i$-dependent gating kinetics of TRPM4 channel before and after application of

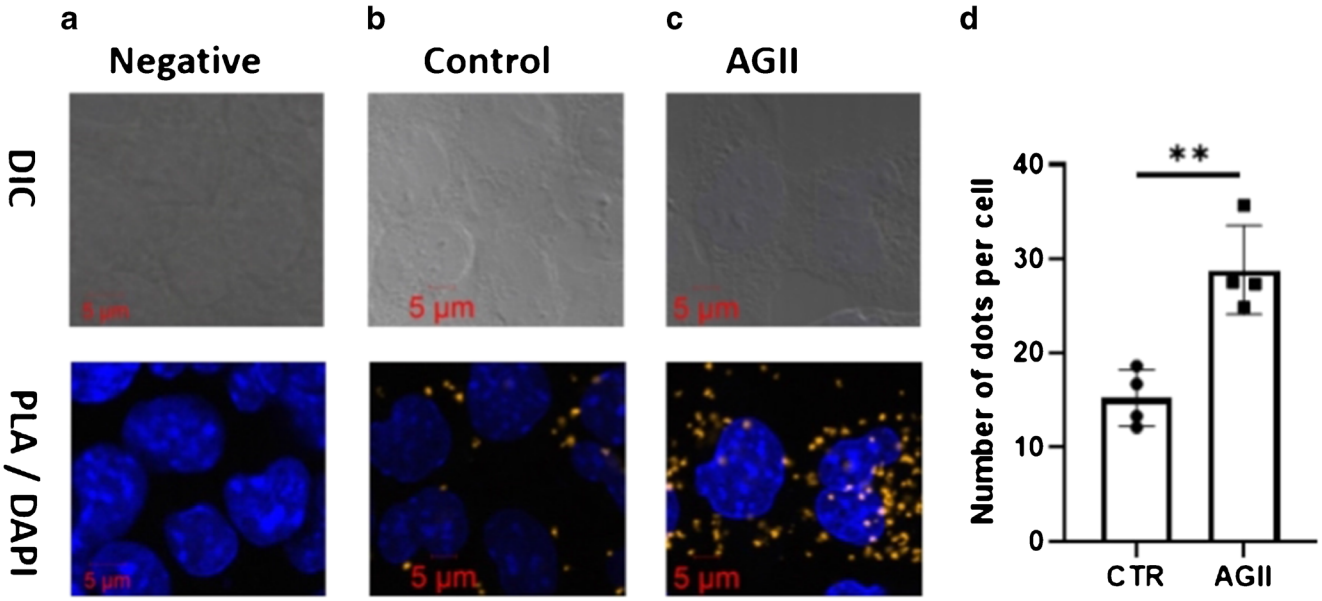

Fig. 3 Close localization of endogenous TRPM4 and CaMKII proteins in HL-1 cells. Representative PLA images from HL-1 cells treated without (**b**) or with (**c**) AGII (1 μM) for 4 days. In the negative control (**a**), primary anti-TRPM4 antibody was omitted. Orange dot signals were generated when endogenous TRPM4 and CaMKII were less than 40 nm. Nuclei are stained blue with DAPI. Scale bars indicate 10 μm. (**d**) Quantitative analysis of the PLA signals. $^{**}p < 0.01$ with upaired *t* test ($n = 4$)

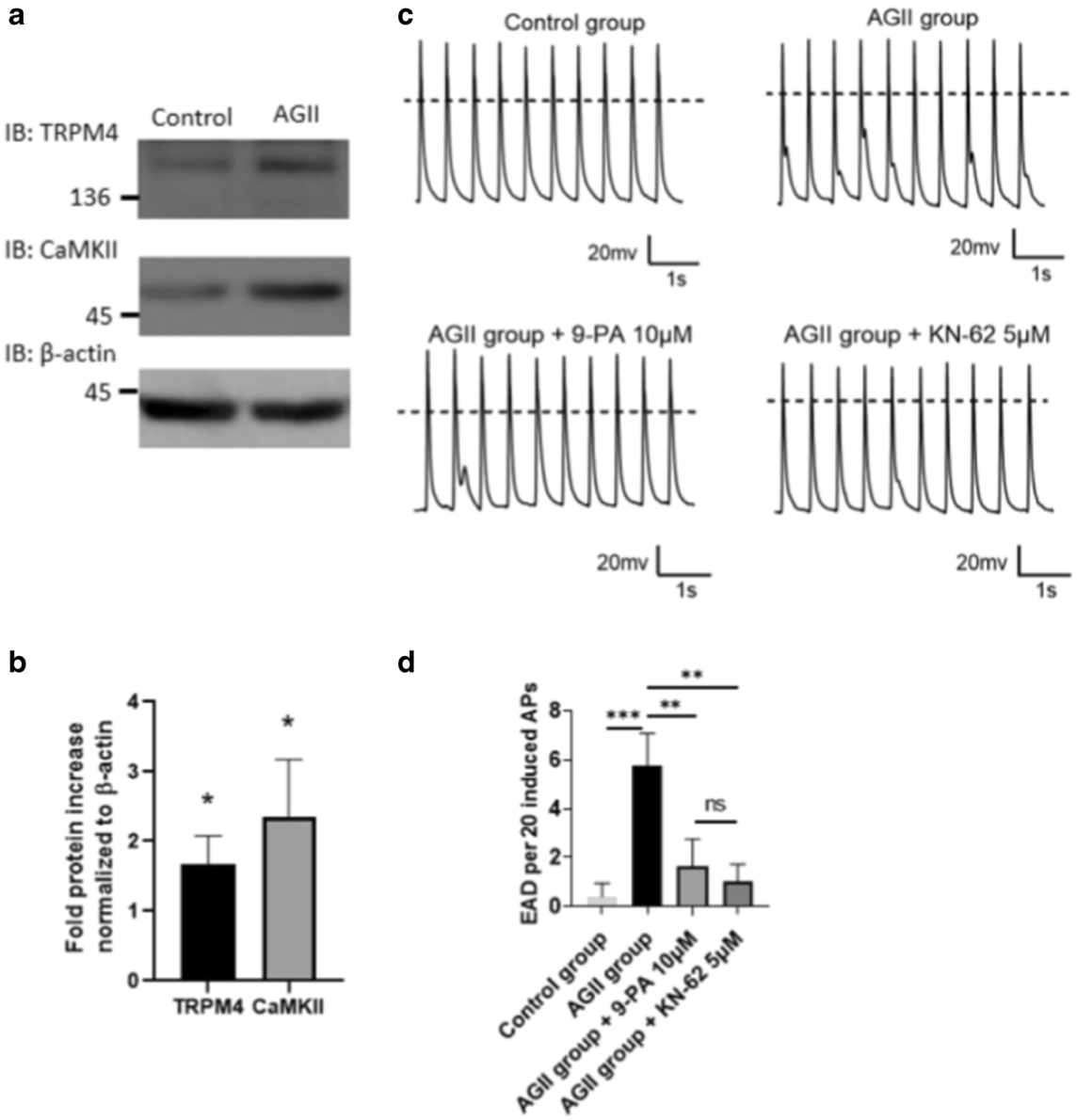

Fig. 4 AGII induces early afterdepolarizations (EADs) with increased expressions of TRPM4 and CaMKII. (**a**) Representative immunoblots of TRPM4, CaMKII, and β-actin proteins (re-probed from the same blot membrane) extracted from non-treated and AGII-treated HL-1 cells. (**b**) Increased expressions of TRPM4 and CaMKII proteins in AGII-treated HL-1 cells. Data are demonstrated as fold changes relative to respective controls (i.e., no AGII treatment) after normalization to β-actin. $*p < 0.05$ with unpaired *t* test ($n = 4$). (**c**) Actual traces of membrane potentials recorded from HL-1 cells in the current clamp mode. AGII treatment induced EADs with 2-Hz pacing (con), which were abolished by 9-PA (10 μM) or KN-62 (5 μM). (**d**) Statistical analysis for EAD occurrence. $***p < 0.001$ and $**p < 0.01$ with ANOVA followed by Tukey's post hoc tests ($n = 5$)

KN-62. The Iono-C/A recording was employed to avoid severe rundown/desensitization. When currents became stable, 5 μM KN-62 was perfused until substantial CaMKII inhibition was attained. It typically required 2–3 min (Fig. 6a).

Figure 6b displays overlaid traces of I_{TRPM4} during and immediately after voltage step pulses in the absence and presence of 5 μM KN-62. The time courses of activation and deactivation in response to each voltage jump were fitted to monoexponentials to get necessary information for the kinetic analysis (not illustrated), as performed previously [16]. At first glance, it is obvious that deactivation of tail TRPM4 currents at the holding potential (− 60 mV) was markedly accelerated after KN-62 application (expanded traces in Fig. 6c). Figure 6 d and e respectively demonstrate averaged relationships of the steady-state open probability (P_o) and time constant of voltage-dependent activation/deactivation (τ) versus membrane potential (V_m) at three different $[Ca^{2+}]_o$ values. $[Ca^{2+}]_i$ values corresponding to respective $[Ca^{2+}]_o$ were separately determined by Ca^{2+} imaging experiments [16]. We adopted a two-state (C-O) transition model with rate constants of

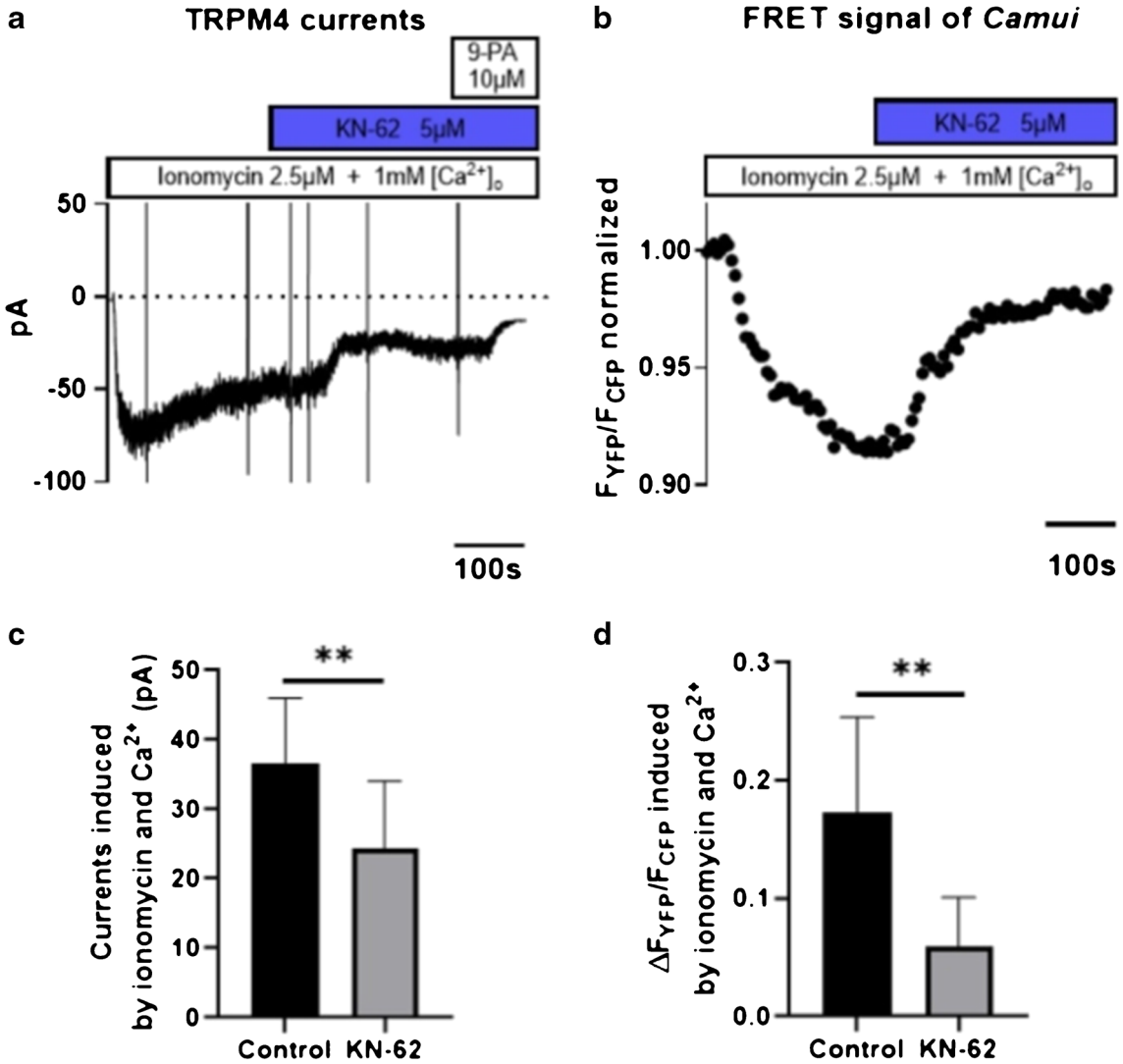

Fig. 5 CaMKII modulates TRPM4 activity through tight coupling. TRPM4 and CaMKIIδ were co-expressed in HEK293 cells and the membrane current was recorded by the ionomycin-permeabilized cell-attached (Iono-C/A) recording. (**a**) Typical development of a TRPM4 current during cumulative administrations of 2.5 μM ionomycin, 1 mM $[Ca^{2+}]_o$ and 5 μM KN-62. (**b**) The CaMKII fluorescent indicator *Camui* was co-expressed together into HEK293 cells. The ratio of fluorescences (F_{YFP}/F_{CFP}) which was normalized to its initial baseline value was obtained under the same experimental conditions as in panel (**a**). (**c**) Averaged TRPM4 currents at − 60 mV. (**d**) The averaged decreases in normalized F_{YFP}/F_{CFP} ($\Delta F_{YFP}/F_{CFP}$) before (control; ionomycin and Ca^{2+} only) and after addition of 5 μM KN-62. In panel (**c**), to avoid potential contamination of leak and other endogenous Ca^{2+}-activated currents, the current remaining after 9-PA application is subtracted to obtain a TRPM4 current as a 9-PA-sensitive component. The effects of Ca^{2+} and KN-62 were evaluated after they reached steady levels. $^{**}p < 0.01$ with paired *t* test, respectively ($n = 5$)

opening and closing α and β to mathematically formulate TRPM4 channel gating before and after application of KN-62 (i.e., CaMKII inhibition), where α and β are the functions of both V_m and Ca^{2+} (Fig. 7a–c and legend). The final mathematical expressions obtained for α and β (in s^{-1}) are:

before application of KN-62:

$$\alpha(V,[\mathrm{Ca}]) = 3.7008 \cdot [\mathrm{Ca}]^{0.17457} \cdot \exp[(0.0071508 - 0.00020179 \cdot [\mathrm{Ca}]) \cdot V]$$
$$\beta(V,[\mathrm{Ca}]) = 0.65836 \cdot \exp\left[(3.5163 - 0.26304 \cdot [\mathrm{Ca}]) + (-0.0045777 - 0.002332 \cdot [\mathrm{Ca}]) \cdot V + (0.0000159 - 0.0000116 \cdot [\mathrm{Ca}]) \cdot V^2\right]$$

after application of KN-62:

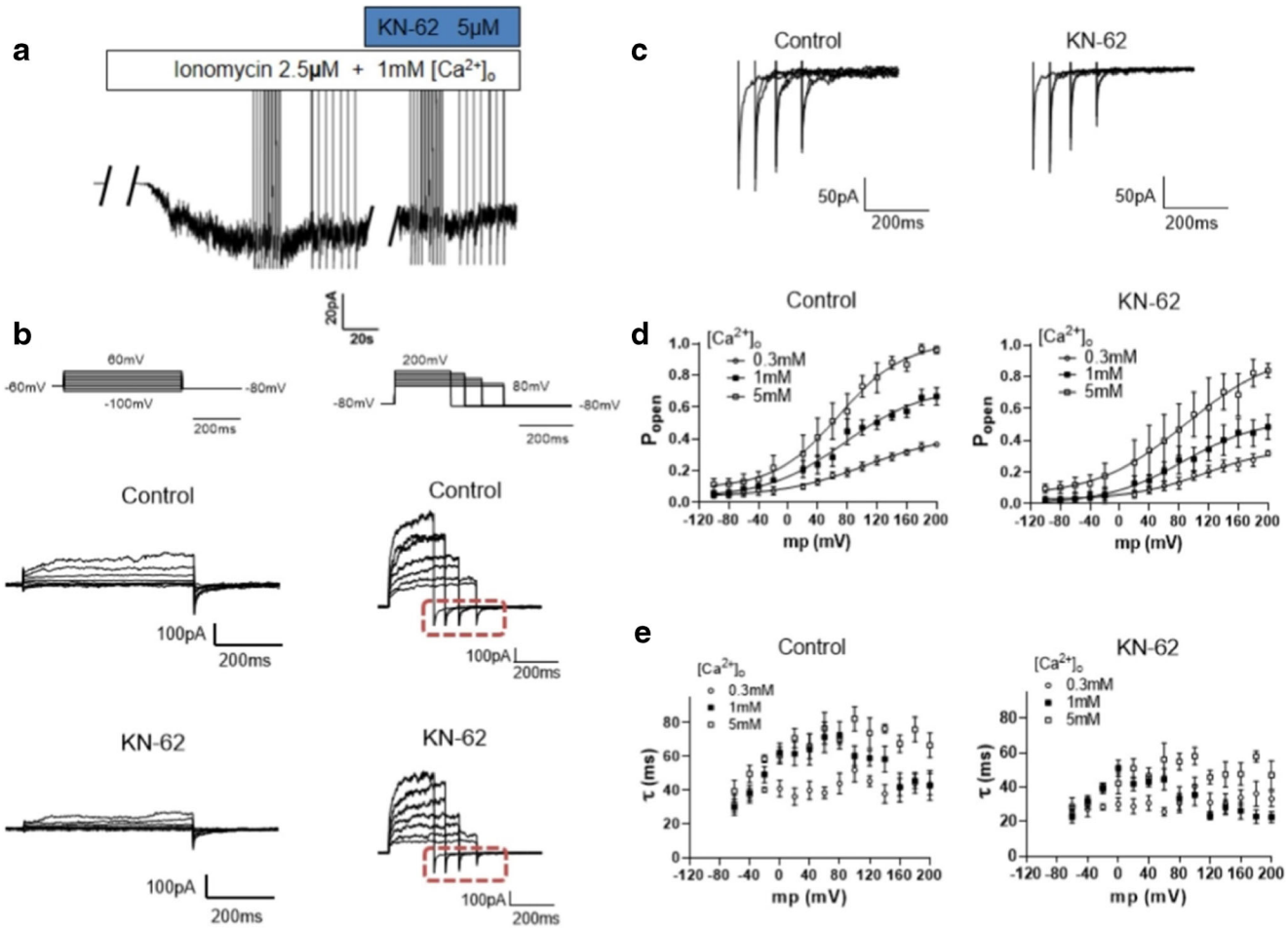

Fig. 6 Voltage jump analyses of Ca^{2+}- and voltage-dependent TRPM4 channel gating. (**a**) The protocol to evaluate Ca^{2+}- and voltage-dependent activation of TRPM4 channel with the I/O cell-attached recording. The details of this method are described elsewhere [16]. Briefly, after the cell membrane was permeabilized by 2.5 μM ionomycin, 0.3, 1, or 5 mM Ca^{2+} was introduced into the bath to induce unitary TRPM4 currents (at the holding potential of − 60 mV), and 5 μM KN-62 was cumulatively applied at least for 2 min. (**b**) Overlaid traces of TRPM4-mediated currents induced by voltage pulses from − 60 mV to − 100 to + 200 mV, before and after application of KN-62. The time constants (τ) for the activation and deactivation of these currents were obtained by mono-exponential fitting. (**c**) Tail TRPM4 currents immediately after the voltage jump are displayed on an expanded scale. (d, e) $[Ca^{2+}]_o$ and voltage dependence of steady-state open probability (P_o) and τ before and after application of KN-62. Symbols represent the averages derived from six selected voltage jump experiments such as shown in panel (**a**). Solid curves in (**d**) are the best fits to the Boltzmann equation: $1/[1 + \exp(-(V_m - V_{0.5})/s)]$, where V_m, $V_{0.5}$, and s denote the membrane potential, half activation voltage, and slope factor, respectively. The best-fit values of $V_{0.5}$ and s are as follows (in mV): for the control, 129.36 and 149.09, 78.39 and 86.18, and 68.44 and 95.52 for 0.3, 1, and 5 mM $[Ca^{2+}]_o$, respectively; for KN-62, 89.96 and 77.8, 62.20 and 51.73, and 60.86 and 73.54 for 0.3, 1, and 5 mM $[Ca^{2+}]_o$, respectively. P_o at 200 mV with 5 mM $[Ca^{2+}]_o$ is assumed to be 1.0 in each voltage jump experiment

$$\alpha(V,[\mathrm{Ca}]) = 1.9469 \cdot [\mathrm{Ca}]^{0.37586} \cdot \exp[(0.010389 - 0.001362 \cdot [\mathrm{Ca}]) \cdot V]$$
$$\beta(V,[\mathrm{Ca}]) = 0.76936 \cdot \exp\left[(3.7267 - 0.2251 \cdot [\mathrm{Ca}]) + (-0.0011664 - 0.0027691 \cdot [\mathrm{Ca}]) \cdot V + (0.00000246 - 0.000000268 \cdot [\mathrm{Ca}]) \cdot V^2\right]$$

where Ca in μM and V in mV.

Numerical AP models reproduce TRPM4- and CaMKII-mediated arrhythmogenic changes

We incorporated the above rate constants into a modified HL-1 evoked AP model (see the "Methods" section) and simulated the impact of CaMKII inhibition on AP generation with 2-Hz pacing. In the absence of CaMKII inhibition, a few-fold increase in TRPM4 current density was sufficient to induce AP prolongation (Fig. 8a). Further increases in TRPM4 current density highly depolarized the diastolic membrane potential and induced EADs (3.25-fold; Fig. 8c) and destabilized AP generation by producing the periodic changes in the shape and pattern

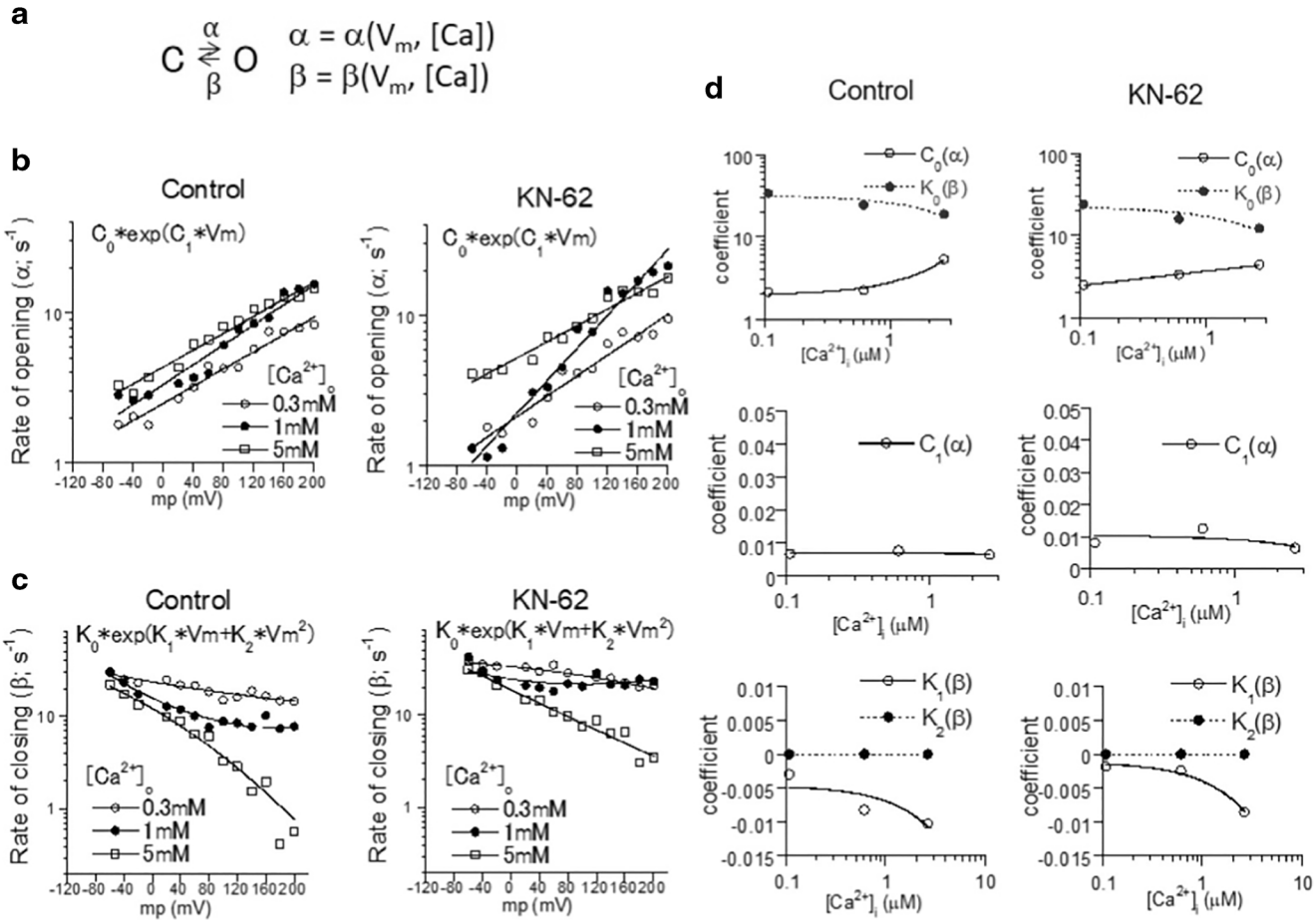

Fig. 7 Mathematical formulation of the Ca^{2+}- and voltage-dependent gating of TRPM4 channel. (**a**) The closed (C)-open (O) state transition model, where α and β are the complex functions of membrane potential (V_m) and Ca^{2+} concentration. (**b**, **c**) Logarithmic plots of α and β against V_m for different $[Ca^{2+}]_o$ before and after application of KN-62. In each voltage jump experiment, the values of α and β were determined, according to the following simultaneous equations: $\tau(V_m) = \frac{1}{\alpha(V_m)+\beta(V_m)}$ $P_o(V_m) = \frac{\alpha(V_m)}{\alpha(V_m)+\beta(V_m)}$ The solid lines are the best nonlinear fits of averaged α and β values before and after application of KN-62 ($n = 6$) by the following exponential functions of V_m with constants C_0, C_1, K_0, K_1 and K_2 for each $[Ca^{2+}]_o$, respectively: $\alpha(V_m) = C_0 \cdot \exp(C_1 \cdot V_m)$ $\beta(V_m) = K_0 \cdot \exp(K_1 \cdot V_m + K_2 \cdot V_m^2)$ (**d**) Plots of C_0, C_1, K_0, K_1, and K_2 against $[Ca^{2+}]_i$. Solid curves are the best fits of each constant's values to either linear, exponential, or power functions of $[Ca^{2+}]_i$. Elevations in $[Ca^{2+}]_i$ induced by various concentrations of $[Ca^{2+}]_o$ during Iono-C/A recording were determined by the Fura-2 fluorescence imaging in separate experiments. The relationship between $[Ca^{2+}]_i$ and $[Ca^{2+}]_o$ was shown in our previous study (Fig. 1 and supplementary Figure 3 in [16])

of EADs (3.5-fold; Fig. 8d). It is noteworthy that similar changes were also recorded from AGII-treated HL-1 cells during the fast pacing of 2 Hz (Fig. 4b). In contrast, after application of KN-62, even the 3.5-fold increase in TRPM4 density could not induce EADs and the extents of diastolic depolarization and AP prolongation due to excessive TRPM4 activation were much more limited (Fig. 8b, d). In addition, the mechanism for EAD generation appears to involve the reactivation of voltage-dependent T-type Ca current, since its temporal change in the magnitude exactly matches up with that of the inward TRPM4 current (middle and bottom traces in Fig. 8c–e).

Discussion

It is well established that CaMKII-dependent phosphorylation greatly alters the gating behaviors of many ion channels associated with AP generation such as voltage-dependent Ca^{2+} and Na^+ channels and ryanodine receptors thereby inducing arrhythmogenicity [10]. In this study, we demonstrated that TRPM4 and CaMKII proteins are closely localized to interact functionally, by use of immunofluorescent confocal microscopy, western blotting, PLA assay, FRET, and electrophysiology. Furthermore, we provided for the first time the evidence in vitro and in silico that when excessive, this interaction can induce arrhythmogenic changes.

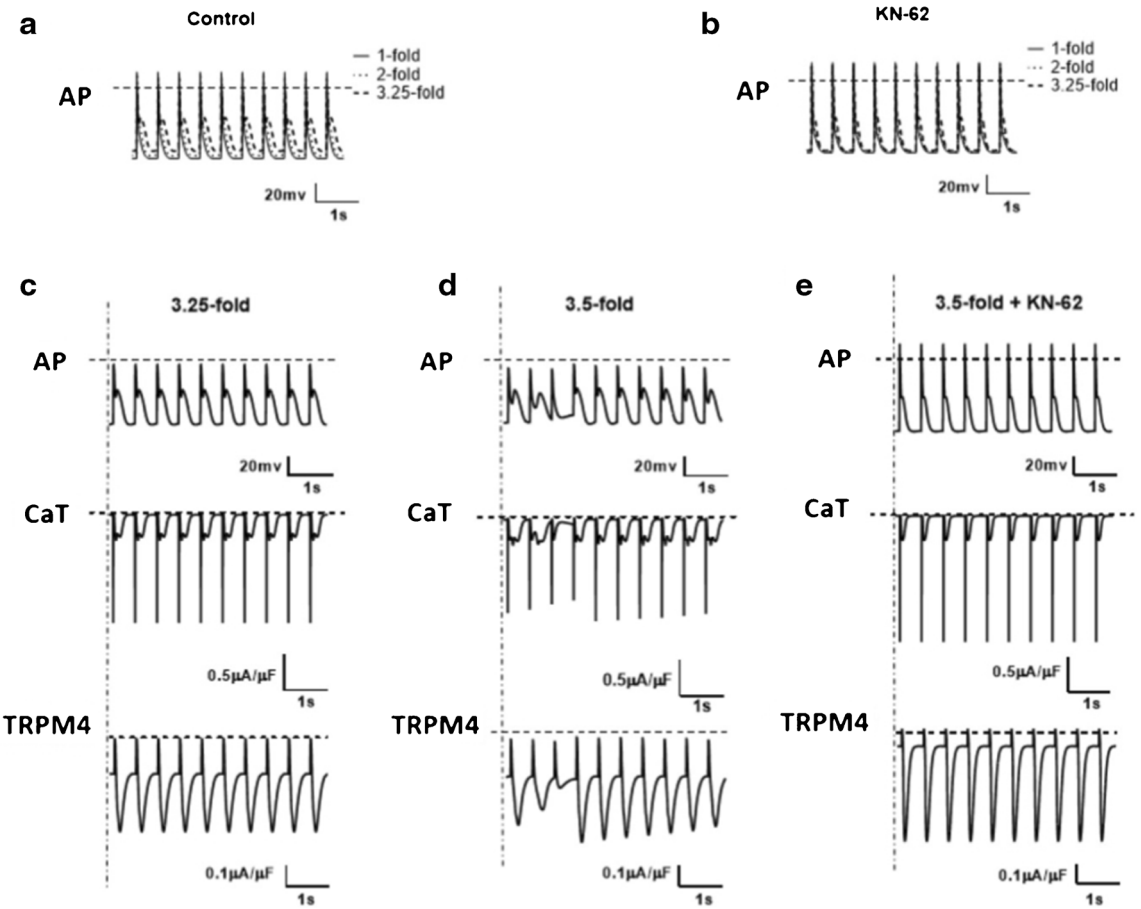

Fig. 8 AP simulation with a modified HL-1 model. (**a**, **b**) A modified HL-1 model incorporating TRPM4 channel (see the "Methods" section) was used to simulate APs evoked by 2-Hz stimulation in the absence (**a**) and presence (**b**) of KN-62. The density of TRPM4 channel is adjusted to normal (1-fold) to several-fold levels and the resultant APs are overlaid. Note that the duration of AP is prolonged by increasing TRPM4 density and that this is greatly inhibited by the application of KN-62. (**c**–**e**) Time courses of APs simulated with the same model as above are displayed for the cases of 3.25-fold (**c**) and 3.5-fold (**d**) increases in TRPM4 density, together with those of T-type Ca (CaT) and TRPM4 currents. For the latter, inhibition of CaMKII by KN-62 completely eliminates EADs (**e**)

TRPM4 is a Ca^{2+}-activated cation channel tightly associated with the intracellular Ca^{2+} homeostasis and dynamics in many distinct types of cells [9]. In the normal heart, this channel is presumed to be essential for pace-making depolarization and β-adrenergic inotropy [13, 23]. However, in the stressed heart, the channel appears to undergo pathological upregulation to cause abnormal diastolic depolarization and AP prolongation [16, 27], both being predisposing factors to cardiac arrhythmias. It is generally thought that considerable part of intracellular Ca^{2+} signaling is mediated by a major Ca^{2+}-binding protein calmodulin (CaM) [4]. Indeed, for TRPM4 channel, several putative CaM-binding sites are predicted and shown to be functionally important for the channel activity by molecular biological and electrophysiological investigations [24]. The new finding of the present study is that CaMKII, the key enzyme at the downstream of Ca^{2+}/CaM signaling, may also be pivotal to TRPM4 channel regulation via tight functional coupling. CaMKII has been suggested to be redox sensitive and involved in cardiac failure and arrhythmias [21]. TRPM4 is also highly expressed in stressed or injured hearts undergoing remodeling changes [11] and activated by ischemic insults [31]. The structural analysis of TRPM4 protein revealed that a disulfide bond adjacent to the glycosylation site of the S6 domain is a possible small-molecule recognition site for redox sensitivity [8]. It is thus plausible that both proteins functionally cooperate and would contribute to a variety of secondary arrhythmias associated with cardiac damage and remodeling.

It is well known that L-type calcium channel, which represents the main route for Ca^{2+} influx into cardiomyocytes, co-localizes with ryanodine receptors in the junctional microdomain to exert the Ca^{2+}-induced Ca^{2+} release [5]. This arrangement is essential for tight functional cooperation between the calcium channel and ryanodine receptor thereby driving the excitation-contraction coupling of the heart. A similar microdomain-dependent interaction was recently proposed in atrial myocytes for shear stress-induced activation of TRPM4 channel via the Ca^{2+} release through the type 2 IP_3

receptor (and subsequent Ca^{2+} release from adjacent ryanodine receptors) from the peripheral junctional SR. Although the exact biological significance of this mechanism remains to be determined, the depolarizing nature of TRPM4 channel activation caused by a local mechanical Ca^{2+} release might provide a previously unidentified link to cardiac abnormal excitability [28]. In an intriguing analogy with these two studies, our confocal immunofluorescence microscopy revealed that TRPM4 and CaMKII proteins endogenously expressed in HL-1 cardiomyocytes were closely localized. Although we did not investigate the exact site(s) of this close localization, it is noteworthy that the maximum magnitude of TRPM4 current measured with EGTA in the pipette was much larger than that with BAPTA (Figure 2 in [16]). Like in L-type Ca^{2+} channel [1], this observation most likely supports the junctional microdomain-dependent colocalization of CaMKII and TRPM4 and their functional coupling, where the much weaker and slower Ca^{2+} chelating ability of EGTA than of BAPTA would hamper the effective buffering of rapid and large $[Ca^{2+}]_i$ elevations caused by the junctional Ca^{2+} release. Moreover, experiments heterologously expressing TRPM4 and CaMKII showed that these two proteins preferentially localized in a close vicinity (within 40 nm; by PLA; Figs. 2 and 3) and tightly interacted in response to $[Ca^{2+}]_i$ elevations (FRET measurements; Fig. 5b, d). Similar results were also obtained by the PLA for endogenously expressed TRPM4 and CaMKII proteins in HL-1 cells. All these findings strongly suggest that tight functional interaction is present between these two proteins. This idea is actually corroborated by the electrophysiological data that pharmacological inhibition of CaMKII reduced the magnitude of TRPM4-mediated current through altered gating kinetics (Figs. 5 and 6). Importantly, the interaction of TRPM4 and CaMKII appeared to become more prominent under stressed conditions (i.e., AGII treatment) that enhanced the expressions of the two proteins and induced arrhythmogenic changes (Fig. 4).

In current clamp recordings from HL-1 cells, upregulation of TRPM4 and CaMKII proteins induced by AGII caused a high incidence of EAD, which was suppressed by both TRPM4 and CaMKII inhibitors (Fig. 4). Since AGII is a major neurohormonal stress promoting cardiac remodeling, it is tempting to speculate that the upregulation (and consequently enhanced interaction) of TRPM4 and CaMKII may serve as an as-yet-unidentified substrate for remodeling-associated arrhythmias. Indeed, numerical simulations based on a modified HL-1 model clearly indicated that only a few-fold increase in TRPM4 density (which really occurred with AGII treatment; e.g., see Fig. 4G in [16]) can induce EADs and further increases cause more complex EAD patterns in varying appearance and amplitude (Fig. 8). Notably, these arrhythmogenic changes were completely abolished by the inhibition of CaMKII with KN-62 (Fig. 8). Consultation with literature confirms that more than 4-fold upregulation of TRPM4 could in fact occur in a cardiac hypertrophy model of SHR [11] as well as in human end-stage heart failures [7], both of which are well known to be pro-arrhythmic. In addition, there is also good evidence that excessive activation of CaMKII is a key cellular event involved in various remodeling-associated arrhythmias [29]. Thus, the abnormally enhanced interaction between TRPM4 and CaMKII (due to their pathological upregulations) may be an important pathogenic mechanism predisposing to remodeling-associated arrhythmias.

After CaMKII inhibition, tail TRPM4 currents immediately after voltage step pulses showed much faster deactivation than those before the inhibition (Fig. 6b, c). We explored the precise implication of this observation by detailed kinetic analyses. As summarized in Supplementary Figure 1, in normal setting, the rate constants of opening (α) and closing (β) in the two-state (C-O) transition model are reciprocally dependent on the membrane potential, i.e., being incremental and decremental with respect to voltage, respectively. However, after CaMKII inhibition (except at very high $[Ca^{2+}]_i$ values), both α and β become poorly sensitive to voltage change, staying at very low and high values, respectively. As a result, the open probability of TRPM4 channel is constantly low over the wide ranges of voltage and $[Ca^{2+}]_i$ and the time course of deactivation is accelerated around the resting membrane potential. These simulation results strongly suggest that voltage-dependent transitions between the closed and open states are critically controlled by a CaMKII-mediated mechanism(s). To seek the generality of this mechanism, we also performed similar simulations with a well-established ventricular AP model (Luo-Rudy 2000) [22]. As shown in Supplementary Figure 2, increasing the TRPM4 channel density prolonged AP duration and ultimately (more than 5.5-fold) triggered EADs. In contrast, the inhibition of CaMKII completely abolished all these arrhythmogenic changes. It should be noted that the same degree of fold increase in TRPM4 channel density appears to make differential impacts on ventricular and atrial AP models. However, at repolarization phase, TRPM4-mediated current is much smaller relative to the sum of outward currents (IKs, IK1, etc.) in ventricular than in atrial cardiomyocytes [18]. From these considerations, for both ventricular and atrial arrhythmias, inhibiting excessive TRPM4 channel activity through CaMKII inhibition might work as a new effective anti-arrhythmic strategy.

In summary, the present study provided several lines of evidence that TRPM4 and CaMKII proteins are closely localized and functionally coupled. Electrophysiological experiments in HL-1 atrial myocyte-like cells indicated that pharmacological CaMKII inhibition greatly suppressed the generation of EADs induced by excessive TRPM4 channel activity. Consistent with this result, numerical simulations and kinetic analyses suggested that CaMKII inhibition can effectively mitigate arrhythmogenic changes via reduced TRPM4 activities and that this likely occurs through eliminating the voltage-

dependent C-O transitions of TRPM4 channel. In conclusion, the present study has presented the utility of combined electrophysiological and numerical approaches to elucidate pleiotropic mechanisms underlying arrhythmogenic changes associated with excessive CaMKII activity in the remodeled heart.

Supplementary Information The online version contains supplementary material available at https://doi.org/10.1007/s00424-020-02507-w.

Availability of data and material (data transparency) The data described and materials used in this paper are available on request.

Authors' contributions Y.H., H.A., and R.I. conceived this study; Y.H. conducted patch clamp experiments and analyzed the obtained data; Y.H., DR.K., M.E., and P.A. contributed immunoblotting, immunofluorescence, and PLA experiments and analyzed the obtained data; R.I. and Y.H. conducted simulations on the HL-1 AP model. T.F. helped to design the work and commented on the draft. Y.H., R.I., and H.A. contributed funding acquisition; Y.H. and R.I. wrote the manuscript and all authors reviewed and commented it.

Funding This work has been supported by a JSPS Grant-in-Aid for Young Scientists (B) (No. 17K15566) to Y.H., a JSPS Grant-in-Aid for Scientific Research (B) (No. 15H04678) to R.I., and Swiss National Science Foundation to H.A. (No. 310030_184783).

Compliance with ethical standards

Conflict of interest Not applicable

Ethics approval Not applicable

Consent to participate All authors confirmed that their roles played in this work are properly appreciated, and approved the order of authorship. The authors gratefully acknowledge Jean-Sébastien Rougier for *constructive* comments during experiments.

Consent for publication All authors agreed to submit/publish this paper after careful reading.

Code availability (software application or custom code) The codes for modified HL-1 models incorporating TRPM4 kinetics with and without CaMKII inhibition (written in CellML) can be provided on request. The original HL-1 model was written in Visual C++ (Takeuchi et al., 2013) which was translated into CellML (by Hu and Inoue). The Luo-Rudy 2000 model is available from the Cor library (Oxford; URL: http://cor.physiol.ox.ac.uk/).

References

1. Adachi-Akahane S, Cleemann L, Morad M (1996) Cross-signaling between L-type Ca^{2+} channels and ryanodine receptors in rat ventricular myocytes. J Gen Physiol 108:435–454
2. Ardestani G, West MC, Maresca TJ, Fissore RA, Stratton MM (2019) FRET-based sensor for CaMKII activity (FRESCA): a useful tool for assessing CaMKII activity in response to Ca^{2+} oscillations in live cells. J Biol Chem 294:11876–11891. https://doi.org/10.1074/jbc.RA119.009235
3. Backs J, Backs T, Neef S, Kreusser MM, Lehmann LH, Patrick DM, Grueter CE, Qi X, Richardson JA, Hill JA (2009) The δ isoform of CaM kinase II is required for pathological cardiac hypertrophy and remodeling after pressure overload. Proc Natl Acad Sci 106:2342–2347
4. Bagur R, Hajnoczky G (2017) Intracellular Ca^{2+} sensing: its role in calcium homeostasis and signaling. Mol Cell 66:780–788. https://doi.org/10.1016/j.molcel.2017.05.028
5. Bers DM (2002) Cardiac excitation-contraction coupling. Nature 415:198–205. https://doi.org/10.1038/415198a
6. Claycomb WC, Lanson NA, Stallworth BS, Egeland DB, Delcarpio JB, Bahinski A, Izzo NJ (1998) HL-1 cells: a cardiac muscle cell line that contracts and retains phenotypic characteristics of the adult cardiomyocyte. P Natl Acad Sci U S A 95:2979–2984. https://doi.org/10.1073/pnas.95.6.2979
7. Dragún M, Gažová A, Kyselovič J, Hulman M, Máťuš M (2019) TRP channels expression profile in human end-stage heart failure. Medicina 55:380
8. Duan J, Li Z, Li J, Santa-Cruz A, Sanchez-Martinez S, Zhang J, Clapham DE (2018) Structure of full-length human TRPM4. Proc Natl Acad Sci U S A 115:2377–2382. https://doi.org/10.1073/pnas.1722038115
9. Gees M, Colsoul B, Nilius B (2010) The role of transient receptor potential cation channels in Ca^{2+} signaling. Cold Spring Harb Perspect Biol 2:a003962. https://doi.org/10.1101/cshperspect.a003962
10. Glynn P, Musa H, Wu XQ, Unudurthi SD, Little S, Qian L, Wright PJ, Radwanski PB, Gyorke S, Mohler PJ, Hund TJ (2015) Voltage-gated sodium channel phosphorylation at Ser571 regulates late current, arrhythmia, and cardiac function in vivo. Circulation 132:567–577. https://doi.org/10.1161/Circulationaha.114.015218
11. Guinamard R, Demion M, Magaud C, Potreau D, Bois P (2006) Functional expression of the TRPM4 cationic current in ventricular cardiomyocytes from spontaneously hypertensive rats. Hypertension 48:587–594. https://doi.org/10.1161/01.HYP.0000237864.65019.a5
12. Heijman J, Voigt N, Nattel S, Dobrev D (2014) Cellular and molecular electrophysiology of atrial fibrillation initiation, maintenance, and progression. Circ Res 114:1483–1499. https://doi.org/10.1161/CIRCRESAHA.114.302226
13. Hof T, Simard C, Rouet R, Salle L, Guinamard R (2013) Implication of the TRPM4 nonselective cation channel in mammalian sinus rhythm. Heart Rhythm 10:1683–1689. https://doi.org/10.1016/j.hrthm.2013.08.014
14. Hof T, Sallé L, Coulbault L, Richer R, Alexandre J, Rouet R, Manrique A, Guinamard R (2016) TRPM4 non-selective cation channels influence action potentials in rabbit Purkinje fibres. J Physiol 594:295–306
15. Hof T, Chaigne S, Recalde A, Salle L, Brette F, Guinamard R (2019) Transient receptor potential channels in cardiac health and disease. Nat Rev Cardiol 16:344–360. https://doi.org/10.1038/s41569-018-0145-2
16. Hu YP, Duan YB, Takeuchi A, Hai-Kurahara L, Ichikawa J, Hiraishi K, Numata T, Ohara H, Iribe G, Nakaya M, Mori MX, Matsuoka S, Ma G, Inoue R (2017) Uncovering the arrhythmogenic potential of TRPM4 activation in atrial-derived HL-1 cells using novel recording and numerical approaches. Cardiovasc Res 113:1243–1255. https://doi.org/10.1093/cvr/cvx117
17. Inoue R, Ito Y (2000) Intracellular ATP slows time-dependent decline of muscarinic cation current in guinea pig ileal smooth muscle. Am J Phys Cell Phys 279:C1307–C1318. https://doi.org/10.1152/ajpcell.2000.279.5.C1307
18. Jeevaratnam K, Chadda KR, Huang CL, Camm AJ (2018) Cardiac potassium channels: physiological insights for targeted therapy. J Cardiovasc Pharmacol Ther 23:119–129. https://doi.org/10.1177/1074248417729880
19. Johannessen CM, Boehm JS, Kim SY, Thomas SR, Wardwell L, Johnson LA, Emery CM, Stransky N, Cogdill AP, Barretina J,

Caponigro G, Hieronymus H, Murray RR, Salehi-Ashtiani K, Hill DE, Vidal M, Zhao JJ, Yang XP, Alkan O, Kim S, Harris JL, Wilson CJ, Myer VE, Finan PM, Root DE, Roberts TM, Golub T, Flaherty KT, Dummer R, Weber BL, Sellers WR, Schlegel R, Wargo JA, Hahn WC, Garraway LA (2010) COT drives resistance to RAF inhibition through MAP kinase pathway reactivation. Nature 468:968–U370. https://doi.org/10.1038/nature09627

20. Lam AJ, St-Pierre F, Gong Y, Marshall JD, Cranfill PJ, Baird MA, McKeown MR, Wiedenmann J, Davidson MW, Schnitzer MJ, Tsien RY, Lin MZ (2012) Improving FRET dynamic range with bright green and red fluorescent proteins. Nat Methods 9:1005–1012. https://doi.org/10.1038/nmeth.2171
21. Luczak ED, Anderson ME (2014) CaMKII oxidative activation and the pathogenesis of cardiac disease. J Mol Cell Cardiol 73:112–116. https://doi.org/10.1016/j.yjmcc.2014.02.004
22. Luo CH, Rudy Y (1994) A dynamic model of the cardiac ventricular action potential. II. Afterdepolarizations, triggered activity, and potentiation. Circ Res 74:1097–1113. https://doi.org/10.1161/01.res.74.6.1097
23. Mathar I, Kecskes M, Van der Mieren G, Jacobs G, Camacho Londoño JE, Uhl S, Flockerzi V, Voets T, Freichel M, Nilius B (2014) Increased β-adrenergic inotropy in ventricular myocardium from Trpm4−/− mice. Circ Res 114:283–294
24. Nilius B, Prenen J, Tang J, Wang C, Owsianik G, Janssens A, Voets T, Zhu MX (2005) Regulation of the Ca^{2+} sensitivity of the nonselective cation channel TRPM4. J Biol Chem 280:6423–6433. https://doi.org/10.1074/jbc.M411089200
25. Sag CM, Mallwitz A, Wagner S, Hartmann N, Schotola H, Fischer TH, Ungeheuer N, Herting J, Shah AM, Maier LS, Sossalla S, Unsold B (2014) Enhanced late INa induces proarrhythmogenic SR Ca leak in a CaMKII-dependent manner. J Mol Cell Cardiol 76:94–105. https://doi.org/10.1016/j.yjmcc.2014.08.016
26. Shy D, Gillet L, Ogrodnik J, Albesa M, Verkerk AO, Wolswinkel R, Rougier JS, Barc J, Essers MC, Syam N, Marsman RF, van Mil AM, Rotman S, Redon R, Bezzina CR, Remme CA, Abriel H (2014) PDZ domain-binding motif regulates cardiomyocyte compartment-specific NaV1.5 channel expression and function. Circulation 130:147–160. https://doi.org/10.1161/CIRCULATIONAHA.113.007852
27. Simard C, Sallé L, Rouet R, Guinamard R (2012) Transient receptor potential melastatin 4 inhibitor 9-phenanthrol abolishes arrhythmias induced by hypoxia and re-oxygenation in mouse ventricle. Br J Pharmacol 165:2354–2364
28. Son MJ, Kim JC, Kim SW, Chidipi B, Muniyandi J, Singh TD, So I, Subedi KP, Woo SH (2016) Shear stress activates monovalent cation channel transient receptor potential melastatin subfamily 4 in rat atrial myocytes via type 2 inositol 1, 4, 5-trisphosphate receptors and Ca^{2+} release. J Physiol 594:2985–3004
29. Swaminathan PD, Purohit A, Hund TJ, Anderson ME (2012) Calmodulin-dependent protein kinase II: linking heart failure and arrhythmias. Circ Res 110:1661–1677. https://doi.org/10.1161/CIRCRESAHA.111.243956
30. Takeuchi A, Kim B, Matsuoka S (2013) The mitochondrial Na^+-Ca^{2+} exchanger, NCLX, regulates automaticity of HL-1 cardiomyocytes. Sci Rep 3:2766
31. Wang J, Takahashi K, Piao H, Qu P, Naruse K (2013) 9-Phenanthrol, a TRPM4 inhibitor, protects isolated rat hearts from ischemia-reperfusion injury. PLoS One 8:e70587. https://doi.org/10.1371/journal.pone.0070587
32. Yang Z, Murray KT (2011) Ionic mechanisms of pacemaker activity in spontaneously contracting atrial HL-1 cells. J Cardiovasc Pharmacol 57:28–36. https://doi.org/10.1097/FJC.0b013e3181fda7c4